Distinguishing spin-orbit coupling and nematic order in the electronic spectrum of iron-based superconductors

Rafael M. Fernandes and Oskar Vafek

Distinguishing spin-orbit coupling and nematic order in the electronic spectrum of iron-based superconductors

Rafael M. Fernandes[1] and Oskar Vafek[2]

[1]*School of Physics and Astronomy, University of Minnesota, Minneapolis 55455, USA*
[2]*National High Magnetic Field Laboratory and Department of Physics,*
Florida State University, Tallahasse, Florida 32306, USA

The low-energy electronic states of the iron-based superconductors are strongly affected by both spin-orbit coupling and, when present, by the nematic order. These two effects have different physical origins, yet they can lead to similar gap features in the electronic spectrum. Here we show how to disentangle them experimentally in the iron superconductors with one Fe plane per unit cell. Although the splitting of the low energy doublet at the Brillouin zone center (Γ-point) can be due to either the spin-orbit coupling or the nematic order, or both, the degeneracy of each of the doublet states at the zone corner (M-point) is protected by the space group symmetry even when spin-orbit coupling is taken into account. Therefore, any splitting at M must be due to lowering of the crystal symmetry, such as due to the nematic order. We further analyze a microscopic tight-binding model with two different contributions to the nematic order: d_{xz}/d_{yz} onsite energy anisotropy and the d_{xy} hopping anisotropy. We find that a precise determination of the former, which has been widely used to characterize the nematic phase, requires a simultaneous measurement of the splittings of the Γ-point doublet and at the two low-energy M-point doublets. We also discuss the impact of twin domains and show how our results shed new light on ARPES measurements in the normal state of these materials.

I. INTRODUCTION

In most iron based superconductors[1], the normal state displays two instabilities: a spin-density wave (SDW) transition at T_{SDW} and an orthorhombic/nematic transition at $T_{\mathrm{nem}} \geq T_{\mathrm{SDW}}$[2]. Angle-resolved photo-emission spectroscopy (ARPES), being sensitive to the electronic energy-momentum dispersion[3], is an attractive tool to probe how these distinct ordered states manifest themselves in the electronic spectrum[4–12]. However, the close proximity of the different electronic energy scales, together with the multi-orbital character of the band structure, render this task non-trivial[13]. For instance, in several iron pnictides, a partial energy gap of about 50 meV reported in optics experiments, and also observed by ARPES at the points where folded and unfolded bands cross, has been attributed to the formation of the metallic SDW order[14–16]. This is of the same order of magnitude as the energy splitting attributed to the tetragonal symmetry-breaking arising from the formation of the orthorhombic/nematic phase[4]. As the system is doped towards its maximum superconducting transition temperature, both gaps decrease[16]. Meanwhile, an atomic-like spin-orbit coupling present in the system gives rise to splittings at the Γ point of the order of 10-30 meV in the band structure[17] without any broken-symmetry[13].

Establishing clear criteria to correctly identify the origin of these spectral features is therefore important to advance our understanding of the normal state of the iron superconductors. In principle, the effects of the SDW order – established independently using neutron scattering – on the electronic spectrum can be unambiguously identified, because, being a commensurate density wave, the lattice translational symmetry-breaking is manifested in a folding of the band structure in the

momentum space. The case of the nematic splitting is however more subtle, because it involves only rotational symmetry-breaking, without the lattice translational symmetry-breaking, and therefore no zone folding. As an illustration, consider the subspace spanned by the d_{xz} and d_{yz} Fe orbitals only. On the one hand, the nematic order breaks the tetragonal symmetry, giving rise to an additional term in the Hamiltonian: $\Delta_{\mathrm{nem}} \sum_{\mathbf{k}\sigma} \left(c^{\dagger}_{xz,\mathbf{k}\sigma} c_{xz,\mathbf{k}\sigma} - c^{\dagger}_{yz,\mathbf{k}\sigma} c_{yz,\mathbf{k}\sigma} \right)$, where the operator $c_{a,\mathbf{k}\sigma}$ destroys an electron at orbital a with momentum $\mathbf{k}$ and spin σ. The result is the splitting between the on-site energies of these two orbitals. On the other hand, the spin-orbit coupling λ_{SOC} mixes the two orbitals, and splits the energy of the resulting admixtures, without breaking the tetragonal symmetry, via the additional term: $i\lambda_{\mathrm{SOC}} \sum_{\mathbf{k}\sigma} \sigma \left(c^{\dagger}_{xz,\mathbf{k}\sigma} c_{yz,\mathbf{k}\sigma} - c^{\dagger}_{yz,\mathbf{k}\sigma} c_{xz,\mathbf{k}\sigma} \right)$. To distinguish these two features experimentally, one could in principle use spin polarized ARPES or use the fact that while Δ_{nem} has a pronounced temperature dependence, λ_{SOC} is expected to be nearly temperature-independent. However, the electronic spectral-function's lifetime, manifested as a broadening of the ARPES data, is also strongly temperature-dependent[18,19], making this procedure challenging.

It is important to keep in mind that the orbital states are not the eigenstates of the electronic Bloch problem[20–23]. At first, one may think that this feature renders the qualitative distinction between the effects of the spin-orbit coupling and the nematic order less transparent. Indeed, any transformation from the $3d$ orbital basis of 2 Fe atoms in the crystallographic unit cell to the band basis requires diagonalizing a 20×20 matrix in the presence of spin-orbit coupling. The size of the matrix is larger if the puckered pnictogen or chalcogen is taken
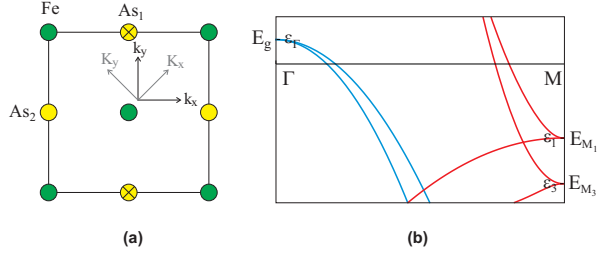
Figure 1: (a) Crystallographic unit cell with 2 Fe atoms. The two coordinate systems (k_x, k_y) and (K_x, K_y) are shown in the figure. (b) Schematic representation of the low-energy model[13] with one doublet E_g at the $\Gamma = (0,0,0)$ point and two doublets E_{M_1} and E_{M_3} at the $M = (\pi, \pi, 0)$ point[24].

into account as well. However, there is an alternative[13]. Because the Fermi pockets are usually small and centered at high-symmetry points of the Brillouin zone, one can focus on the band basis states *directly* at the high symmetry points. Using the properties of the space-group representations near these points, we can qualitatively distinguish the spectral manifestations of spin-orbit coupling and the nematic splitting, sidestepping the need to analyze large matrices.

To this end, we use the effective low-energy model derived using the group-theoretical arguments[13] in the vicinity of $\Gamma = (0,0,0)$ and $M = (\pi, \pi, 0)$ points of the crystallographic Brillouin zone. Focusing on the iron superconductors with tetragonal $P4/nmm$ symmetry group, such as the 11 (FeSe, FeTe), the 111 (NaFeAs, LiFeAs) and the 1111 (LaFeAsO, CeFeAsO) families, and in the presence of time-reversal symmetry, this model features one doublet at Γ, from which two hole pockets originate, and two doublets at M, from which the two electron pockets originate[24] (see Fig. 1). We find that while the doublet at Γ is split by both spin-orbit coupling[13] and nematic order, the two doublets at M are split only by the nematic order. Indeed, without nematic order, the doublets at the M point are guaranteed[13], because each transforms as a single four-dimensional double-valued irreducible representation of the space group $P4/nmm$ (see Ref.[25]). This result, being a consequence of the space group symmetry, is general. Our additional analysis using the ten-orbital tight-binding model derived from *ab initio* calculations of Ref.[26] shows that one of the doublets at M is most affected by the on-site energy difference between the d_{xz} and d_{yz} orbitals, and the other doublet at M by the anisotropy in the hopping parameter connecting the d_{xy} orbitals of neighboring Fe atoms. Because all three quantities contribute to the splittings of the three doublets, it is necessary to simultaneously measure the three splittings in ARPES experiments in order to unambiguously disentangle the effects of nematicity and the spin-orbit coupling. Finally, we discuss the role played by twin domains and the applicability of our results to the 122 family of iron superconductors with $I4/mmm$ space-group symmetry, such as $BaFe_2As_2$.

The paper is organized as follows: in Section II we

introduce the low-energy model in the presence of both spin-orbit coupling and nematic order, and discuss the corresponding band dispersions. In Section III we compare these results to first-principle calculations fitted to a 10-orbital tight-binding model, and to ARPES experiments. Conclusions are presented in Section IV.

II. EFFECTIVE LOW-ENERGY MODEL

The low energy effective Hamiltonian for the states near the Fermi level, corresponding to small hole-like and electron-like pockets, can be obtained from the **k.p** expansion around the Γ and M points of the crystallographic Brillouin zone, which contains 2 Fe atoms[13]. A schematic representation of the corresponding unit cell is shown in Fig. 1a; hereafter, xy refer to the Fe-As orthogonal directions (parallel to the crystallographic ab axes), whereas XY refer to the Fe-Fe orthogonal directions. Here, we focus on the $k_z = 0$ plane only, since ARPES measurements have enough resolution to select single k_z values via the energy of the incoming photon[8]. All the orbitals are defined with respect to the Fe-Fe square lattice, i.e. in the notation d_{xz}, d_{yz}, d_{xy}, $d_{x^2-y^2}$, $d_{3z^2-r^2}$ the subscripts should be understood as referring to the XY coordinate system.

At Γ, the irreducible representations of the $P4/nmm$ space group, suitable for the systems with a single Fe layer per unit cell (i.e. the 11, 111, and 1111 families) are the same as those of the well known point group D_{4h}. Two hole pockets emerge from the E_g doublet, at an energy $\epsilon_\Gamma > 0$, which has degenerate d_{xz}/d_{yz} orbital character (for convenience, we set the chemical potential to zero). Additional hole pockets may or may not emerge from the singlets A_{1g} (with $d_{3z^2-r^2}$ orbital character) and B_{1g} (with d_{xy} character), depending on their position relative to the Fermi level. Because the main qualitative changes caused by the nematic order and the spin-orbit coupling occur in the degenerate states, we focus on the states arising from the E_g doublet only. For each spin projection, σ, we denote them by a two component spinor $\psi_{\Gamma,\sigma}(\mathbf{k})$.

In contrast, at the M point, the irreducible representations of the space group cannot be mapped onto those of the point group D_{4h}. This is a consequence of the fact that $P4/nmm$ is a non-symmorphic space group, due to the presence of an n-glide plane symmetry, i.e. mirror reflection about the Fe plane followed by the translation by the half unit cell diagonal[13]. Ignoring the spin degeneracy, one finds that all irreducible representations at M are two-dimensional, denoted by E_M in Ref.[13]. The two electron pockets arise from the doublet E_{M_1}, at an energy $\epsilon_1 < 0$ and with d_{xz}/d_{yz} orbital character, and from the doublet E_{M_3}, at an energy $\epsilon_3 < \epsilon_1 < 0$ and with d_{xy} orbital character (see Fig. 1b). Out of these 4 states we build two spinors $\psi_{X,\sigma}(\mathbf{k})$ and $\psi_{Y,\sigma}(\mathbf{k})$, whose upper (lower) components transform respectively as $E_{M_1}^X$ and $E_{M_1}^Y$ ($E_{M_3}^X$ and $E_{M_3}^Y$). A schematic representation of

these states is shown in Fig. 1.

Defining the enlarged spinor $\Psi_\sigma^\dagger = \left(\psi_{X,\sigma}^\dagger \ \ \psi_{Y,\sigma}^\dagger \ \ \psi_{\Gamma,\sigma}^\dagger \right)$, the low-energy Hamiltonian can be written as

$$\mathcal{H} = \sum_{\mathbf{k}\alpha\beta} \Psi_\alpha^\dagger(\mathbf{k}) H_{\alpha\beta}(\mathbf{k}) \Psi_\beta(\mathbf{k}), \tag{1}$$

where (suppressing α, β and $\mathbf{k}$) the matrix

$$H = H_0 + H_{\text{SOC}} + H_{\text{nem}}, \tag{2}$$

is the single-particle Hamiltonian in the nematic-paramagnetic state. The first two terms were obtained in Ref.[13] and we repeat here the results. For the non-interacting H_0 part, we obtain:

$$H_0(\mathbf{k}) = \begin{pmatrix} h_M^+(\mathbf{k}) & 0 & 0 \\ 0 & h_M^-(\mathbf{k}) & 0 \\ 0 & 0 & h_\Gamma(\mathbf{k}) \end{pmatrix} \otimes \sigma_0, \tag{3}$$

with 2×2 matrices:

$$h_M^\pm(\mathbf{k}) = \sum_{i=1,3} \left(\epsilon_i + \frac{k^2}{2m_i} \pm a_i k_x k_y \right) \tilde{\tau}_i + v_\pm(\mathbf{k}) \tau_2,$$

$$h_\Gamma(\mathbf{k}) = \left(\epsilon_\Gamma + \frac{k^2}{2m_\Gamma} \right) \tau_0 + b k_x k_y \tau_3 + c \left(k_x^2 - k_y^2 \right) \tau_1, \tag{4}$$

where $\tilde{\tau}_1 = \frac{1}{2}(\tau_0 + \tau_3)$, $\tilde{\tau}_3 = \frac{1}{2}(\tau_0 - \tau_3)$, and:

$$v_\pm(\mathbf{k}) = v(\pm k_x + k_y) + p_1(\pm k_x^3 + k_y^3) + p_2 k_x k_y (k_x \pm k_y) \tag{5}$$

The Pauli matrices σ refer to the spin space, whereas the Pauli matrices τ refer to the spinor space. The simplicity and generality of this model should be evident when compared to the 10-orbital tight-binding model with fifth-neighbor hopping parameters. The 13 free parameters are material-dependent, and can be fit to first-principle calculations. For concreteness, in this paper we use the parameters defined in the first row of Table IX of Ref.[13]. The corresponding band dispersions and Fermi surfaces are shown as dashed lines in Fig. 2. For the spin-orbit term H_{SOC} we have:

$$H_{\text{SOC}}(\mathbf{k}) = \begin{pmatrix} 0 & h_M^{\text{SOC}}(\mathbf{k}) & 0 \\ (h_M^{\text{SOC}})^\dagger(\mathbf{k}) & 0 & 0 \\ 0 & 0 & h_\Gamma^{\text{SOC}}(\mathbf{k}) \end{pmatrix}, \tag{6}$$

with 4×4 matrices:

$$h_M^{\text{SOC}}(\mathbf{k}) = i\frac{\lambda}{4}(\tau_+ \otimes \sigma_1 + \tau_- \otimes \sigma_2),$$

$$h_\Gamma^{\text{SOC}}(\mathbf{k}) = \frac{\lambda}{2} \tau_2 \otimes \sigma_3, \tag{7}$$

and using the usual definition $\tau_\pm = \tau_1 \pm i\tau_2$. Here, λ sets the strength of the spin-orbit coupling, which, without loss of generality, we take to be the same near Γ and M.

To derive the nematic term H_{nem}, which breaks the tetragonal symmetry along the Fe-Fe directions, it is enough to find combinations of components of $\Psi_\sigma(\mathbf{k})$ and $\mathbf{k}$, which transform as B_{2g} invariants, i.e. as $k_x k_y \propto K_x^2 - K_y^2$. Clearly, there can be no bilinear terms which mix the two-component spinors at Γ and M, because such terms would break the lattice translational symmetry. Meanwhile, nematic is a $\mathbf{q} = 0$ order. The $\mathbf{k}$ independent terms near Γ follow immediately from the form of $h_\Gamma(\mathbf{k})$: the only combination of the two components of $\psi_{\Gamma,\sigma}$ which transform as $k_x k_y$ is the combination which multiplies this term in $h_\Gamma(\mathbf{k})$, because the resulting combination is an invariant, i.e. transforms trivially. Therefore, near Γ, the nematic order induces a $\mathbf{k}$-independent term $\sim \sum_{\mathbf{k},\sigma} \psi_{\Gamma,\sigma}^\dagger(\mathbf{k}) \tau_3 \psi_{\Gamma,\sigma}(\mathbf{k})$. Similarly, at M, the $\mathbf{k}$-independent combinations which transform as B_{2g} can be read off from $h_M^\pm(\mathbf{k})$. The two independent terms are $\sim \sum_{\mathbf{k},\sigma} \left(\psi_{X,\sigma}^\dagger(\mathbf{k}) \tilde{\tau}_i \psi_{X,\sigma}(\mathbf{k}) - \psi_{Y,\sigma}^\dagger(\mathbf{k}) \tilde{\tau}_i \psi_{Y,\sigma}(\mathbf{k}) \right)$, where $i = 1$ or $i = 3$. We then obtain

$$H_{\text{nem}}(\mathbf{k}) = \begin{pmatrix} h_M^{\text{nem}}(\mathbf{k}) & 0 & 0 \\ 0 & -h_M^{\text{nem}}(\mathbf{k}) & 0 \\ 0 & 0 & h_\Gamma^{\text{nem}}(\mathbf{k}) \end{pmatrix} \otimes \sigma_0, \tag{8}$$

with 2×2 matrices:

$$h_M^{\text{nem}}(\mathbf{k}) = \frac{\varphi_1}{4}(\tau_0 + \tau_3) + \frac{\varphi_3}{4}(\tau_0 - \tau_3),$$

$$h_\Gamma^{\text{nem}}(\mathbf{k}) = \frac{\varphi_\Gamma}{2} \tau_3. \tag{9}$$

Symmetry alone is unable to fix the values of φ_j. Nevertheless, because all φ_j's are nematic order parameters, they must be related to each other microscopically, although they do not need to be *equal* to each other. It is now straightforward to obtain the electronic spectrum in the presence of both nematic order and spin-orbit coupling. We find splittings in the E_g doublet at the Γ point (energy $\epsilon_\Gamma > 0$), as well as in the E_{M_1} and E_{M_3} doublets at the M point (energies $0 < \epsilon_1 < \epsilon_3$), given by:

$$\Delta E_g = \sqrt{\lambda^2 + \varphi_\Gamma^2}$$

$$\Delta E_{M_{1/3}} = \pm \left(\frac{\varphi_1 - \varphi_3}{2} \right) - \frac{1}{2}\sqrt{\lambda^2 + \left(\epsilon_1 - \epsilon_3 - \frac{\varphi_1 + \varphi_3}{2} \right)^2}$$

$$+ \frac{1}{2}\sqrt{\lambda^2 + \left(\epsilon_1 - \epsilon_3 + \frac{\varphi_1 + \varphi_3}{2} \right)^2}. \tag{10}$$

To make the expressions of the splittings at the M point more transparent, it is useful to consider an expansion in
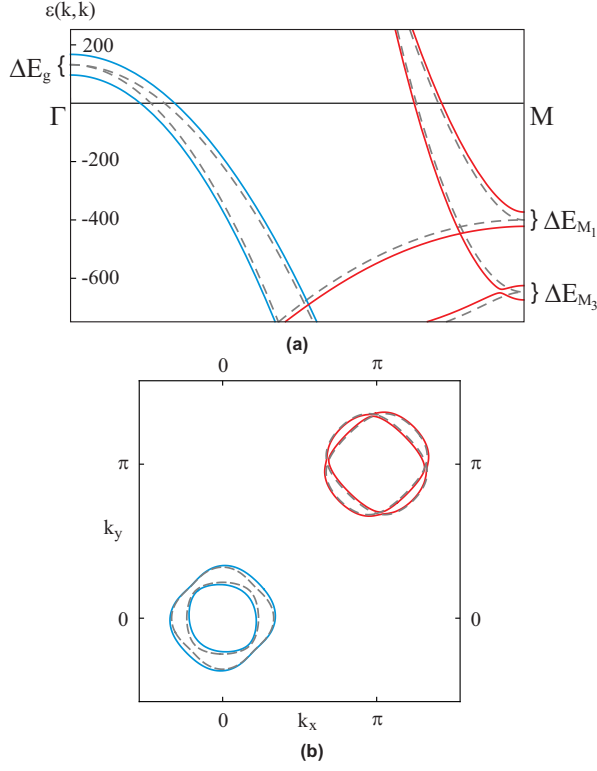
Figure 2: (a) Band dispersion along the Γ-M line in units of meV and (b) Fermi surface of the effective low-energy model in the presence (solid lines) and in the absence (dashed lines) of both spin-orbit coupling and nematic order (solid lines). Red (blue) lines denote the states emerging from the M (Γ) doublets, which will give rise to electron (hole) pockets. The doublet splittings are explicitly shown. In this figure, the parameters used were $\lambda = \varphi_i = 50$ meV.

powers of φ:

$$\Delta E_g = \sqrt{\lambda^2 + \varphi_\Gamma^2},$$

$$\Delta E_{M_1} = \varphi_1 - \frac{(\varphi_1 + \varphi_3)\lambda^2}{4(\epsilon_1 - \epsilon_3)^2} + \mathcal{O}\left(\lambda^2\varphi^3\right),$$

$$\Delta E_{M_3} = \varphi_3 - \frac{(\varphi_1 + \varphi_3)\lambda^2}{4(\epsilon_1 - \epsilon_3)^2} + \mathcal{O}\left(\lambda^2\varphi^3\right). \quad (11)$$

These splittings, the corresponding band dispersions, and the Fermi surface distortions are shown as solid lines in Fig. 2. The fact that the splitting of the high-symmetry doublets are not simply proportional to the nematic order parameter, but depend also on the spin-orbit coupling, is one of our main results. Eq. (11) shows that the E_g doublet at the Γ point can be split by spin-orbit coupling even without tetragonal symmetry-breaking. Moreover, the splitting is insensitive to the sign of the nematic order parameter φ_Γ. We also note that the E_M doublets at the M point can only be split by nematic order. However, once they are split, the spin-orbit coupling also contributes to the splitting, and the magnitude of this contribution depends also on the proximity between the un-

perturbed doublets, $|\epsilon_1 - \epsilon_3|$. Furthermore, while $\varphi_1 \neq 0$ gives the dominant splitting of E_{M_1}, φ_3 can also cause a splitting in E_{M_1} even if $\varphi_1 = 0$, as long as the spin-orbit coupling is non-zero.

Interestingly, the most prominent manifestations of nematic order and spin-orbit coupling on the Fermi surface occur in different pockets (Fig. 2). On the one hand, nematic order has a stronger effect on the hole pockets, as $\varphi_\Gamma > 0$ ($\varphi_\Gamma < 0$) causes the two hole pockets to "repel" each other predominantly along the K_x (K_y) direction. On the other hand, spin-orbit coupling avoids the crossing between the two electron pockets, giving rise to two separate pockets. We emphasize again, despite the presence of spin-orbit coupling and the nematic order parameter, all bands remain doubly-degenerate due to the presence of time reversal and a center of space inversion[13,24].

III. COMPARISON TO FIRST-PRINCIPLE CALCULATIONS AND ARPES EXPERIMENTS

The results derived above are general and independent of the particularities of the band structure. They rely only on the space group symmetry $P4/nmm$ and its consequences at the doublets at Γ and M. Yet, in order to understand the microscopic meaning of the nematic order parameters $(\varphi_\Gamma, \varphi_1, \varphi_3)$, it is instructive to compare our results with those obtained from 10-orbital tight-binding models fitted to first-principle calculations. We used the model of Ref.[26] for LaFeAsO[27] and added two different tetragonal symmetry-breaking terms, while ignoring the spin-orbit coupling. The first is a uniform onsite energy splitting between the d_{xz} and d_{yz} orbitals of the form:

$$H_1 = \frac{\Delta_1}{2}\sum_{\mathbf{k}\sigma}\left(c^\dagger_{xz,\mathbf{k}\sigma}c_{xz,\mathbf{k}\sigma} - c^\dagger_{yz,\mathbf{k}\sigma}c_{yz,\mathbf{k}\sigma}\right), \quad (12)$$

whereas the second is a hopping anisotropy between the d_{xy} orbitals of the two Fe atoms living in the same unit cell:

$$H_3 = \frac{\Delta_3}{2}\sum_{\mathbf{k}\sigma}c^\dagger_{xy(1),\mathbf{k}\sigma}c_{xy(2),\mathbf{k}\sigma}\sin\left(\frac{k_x}{2}\right)\sin\left(\frac{k_y}{2}\right). \quad (13)$$

The results shown in Fig. 3 for $\Delta_1 > 0$, $\Delta_3 = 0$ and $\Delta_1 = 0$, $\Delta_3 > 0$ reveal that whereas the E_g and the E_{M_1} doublets are split by Δ_1, the E_{M_3} doublet is split by Δ_3, with $\Delta E_g = \Delta E_{M_1} = \Delta_1$ and $\Delta E_{M_3} = \Delta_3$. This is not unexpected, since in our low-energy model the E_g and E_{M_1} doublets have d_{xz}/d_{yz} characters, whereas the E_{M_3} doublet has d_{xy} character[13]. Therefore, we can identify $\varphi_\Gamma = \varphi_1$ with the on-site d_{xz}/d_{yz} orbital anisotropy Δ_1 and φ_3 to the d_{xy} hopping anisotropy Δ_3. Note that these results are insensitive to the microscopic mechanism behind the tetragonal symmetry breaking, i.e. whether it arises due to orbital[28–35] or spin fluctuations[2,36–40], or electron-phonon coupling.
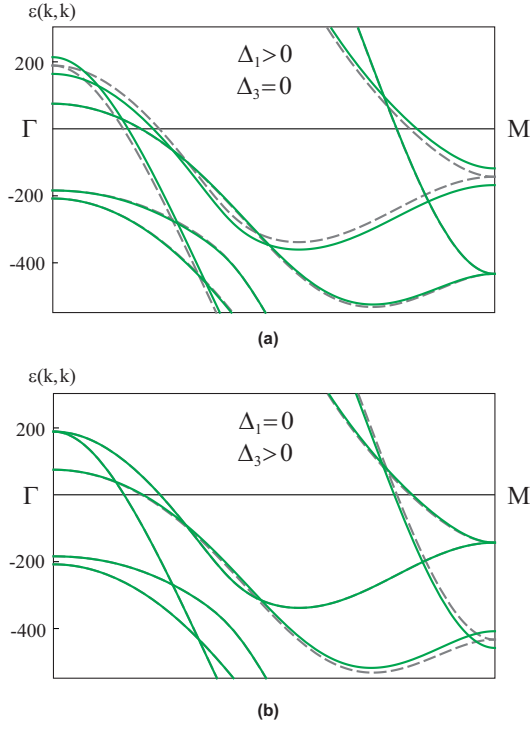
(a)

(b)

Figure 3: Band dispersion along the Γ-M direction (in meV) for the 10-orbital model of Ref.[26] in the presence of (a) an onsite energy anisotropy between the d_{xz}/d_{yz} orbitals, $\Delta_1 = 50$ meV, and (b) a hopping anisotropy between d_{xy} orbitals of nearest-neighbor Fe atoms, $\Delta_3 = 50$ meV. Dashed lines represent the dispersions for $\Delta_1 = \Delta_3 = 0$.

In making quantitative comparison with experiments, an important issue is the presence of twin domains, i.e. while certain regions of the sample are characterized by a set of nematic order parameters $(\varphi_\Gamma, \varphi_1, \varphi_3)$, other regions display $(-\varphi_\Gamma, -\varphi_1, -\varphi_3)$. To take this effect into account, in Fig. 4 we superimpose the band dispersions of the two different types of domains using our effective model of the previous Section. Since ARPES averages over the entire sample, in principle it should be capable of observing the two sets of band dispersions as long as the momentum and energy resolutions are large enough. As expected from symmetry considerations, and confirmed by Eq. (11), the magnitudes of the splittings are insensitive to the sign of the nematic order parameters. In contrast, the band dispersions away from the high-symmetry points are different for distinct domains, resulting in an effective doubling of the number of bands – even though the translational symmetry is not lowered. Remarkably, the hole-pockets dispersions are very similar for the two domain types, reflecting the dependence of the E_g splitting on φ_Γ^2. Thus, depending on the ARPES resolution, it may be difficult to resolve the different domain contributions near the Γ point. Meanwhile, the electron-pockets dispersions are strongly dependent on the sign of φ_1 and φ_3. In particular, for one sign of the nematic order parameter, the two branches dispersing from a given E_{M_i}
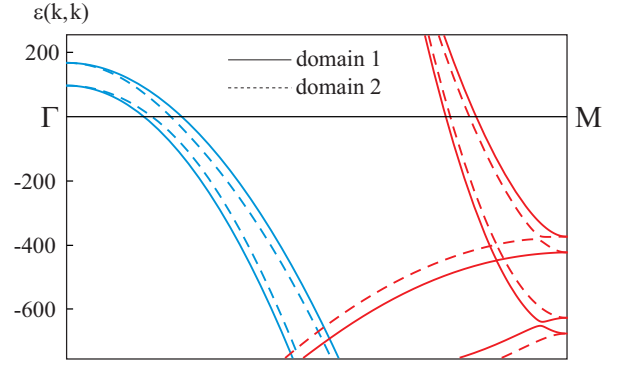

Figure 4: Band dispersions along the Γ-M direction (in meV) for two different types of nematic domain. Solid (dashed) lines correspond to the domain with $\varphi_i = 50$ meV ($\varphi_i = -50$ meV). In both cases, $\lambda = 50$ meV.

doublet either "attract" or "repel" each other – although spin-orbit coupling in general leads to avoided level crossing. As a result, it is more likely for ARPES to be able to resolve the two domains contributions near the M point.

We can now discuss the implications of our results to the interpretation of ARPES experiments in the nematic-paramagnetic state, which takes place in the temperature range $T_{SDW} < T < T_{nem}$ for unstrained samples and in the temperature range $T_{SDW} < T$ for detwinned samples[4–12]. The observed splitting of the E_{M_1} doublet has been mostly attributed to an anisotropy in the onsite energies of the d_{xz} and d_{yz} orbitals (ferro-orbital order), which in our model is given by $\varphi_\Gamma = \varphi_1$. However, our results in Eq. (11) show that this splitting depends also on the nematic order parameter φ_3, corresponding to anisotropic d_{xy} hopping, and on the spin-orbit coupling λ. Thus, to properly disentangle these three contributions $\varphi_1 = \varphi_\Gamma$, φ_3, and λ we argue that it is necessary to measure simultaneously the splitting of the two doublets at the M point and of the doublet at the Γ point. The interplay between these three parameters may also explain why the doublet splittings are different at these two high-symmetry points, as observed experimentally[16].

Applied to twin samples, our results reveal important distinctions in the twin-domains dispersions near the Γ and M points, as shown in Fig. 4. Specifically, while at Γ the dispersions are very similar for the two twin domains, at M they are significantly different, since only in the latter the nematic order gives rise to a bonding and an anti-bonding orbital mixing. Moreover, the doubling of the number of bands is not a consequence of translational symmetry-breaking, since the nematic order is a $\mathbf{q} = 0$ order.

Finally, we comment on the application of our results to the 122 materials, whose space group is $I4/mmm$ instead of $P4/nmm$. In contrast to the latter, the former space group is symmorphic[13]. In the limit of no coupling between the Fe layers, this distinction is irrelevant, and the results derived here for the 1111, 111, and 11 families would also apply to the 122 family. Turning on a weak

inter-layer coupling should lead to small changes, mixing states at $k_z = \pi$ to $k_z = 0$. Although such an additional mixing could complicate the analysis proposed here, it remains to be seen whether it can be resolved by current ARPES experiments.

IV. CONCLUSIONS

In summary, we used a low-energy model that respects all symmetries of the $P4/nmm$ iron superconductors to reveal the interplay between nematic order and spin-orbit coupling in the electronic spectrum of these materials. The simple expressions obtained for the splittings of the three doublets located at the high-symmetry points of the crystallographic Brillouin zone, Eq. (11), enables one to distinguish unambiguously using ARPES experiments

not only these two physical effects, but also the two different contributions to the nematic order – namely the d_{xz}/d_{yz} orbital and d_{xy} hopping anisotropies. These criteria to disentangle spin-orbit and nematicity, being independent of details of the band dispersions, open an interesting route to systematically study the energy scales and the relevance of these two physical effects to the normal state of different iron-based superconductor families.

[1] K. Ishida, Y. Nakai and H. Hosono, J. Phys. Soc. Japan **78**, 062001 (2009); D. C. Johnston, Adv. Phys. **59**, 803 (2010); J. Paglione and R. L. Greene, Nature Phys. **6**, 645 (2010); P. C. Canfield and S. L. Bud'ko, Annu. Rev. Cond. Mat. Phys. **1**, 27 (2010); H. H. Wen and S. Li, Annu. Rev. Cond. Mat. Phys. **2**, 121 (2011).

[2] R. M. Fernandes, A. V. Chubukov, and J. Schmalian, Nature Phys. **10**, 97 (2014).

[3] A. Damascelli, Z. Hussain, and Z.-X. Shen, Rev. Mod. Phys. **75**, 473 (2003).

[4] M. Yi et al., PNAS **108**, 6878 (2011).

[5] Y. Zhang, C. He, Z. R. Ye, J. Jiang, F. Chen, M. Xu, Q. Q. Ge, B. P. Xie, J. Wei, M. Aeschlimann, X. Y. Cui, M. Shi, J. P. Hu, and D. L. Feng, Phys. Rev. B **85**, 085121 (2012).

[6] M. Yi, D. H. Lu, R. G. Moore, K. Kihou, C.-H. Lee, A. Iyo, H. Eisaki, T. Yoshida, A. Fujimori, and Z.-X. Shen, New J. Phys. **14**, 073019 (2012).

[7] T. Shimojima, T. Sonobe, W. Malaeb, K. Shinada, A. Chainani, S. Shin, T. Yoshida, S. Ideta, A. Fujimori, H. Kumigashira, K Ono, Y. Nakashima, H. Anzai, M. Arita, A. Ino, H. Namatame, M. Taniguchi, M. Nakajima, S. Uchida, Y. Tomioka, T. Ito, K. Kihou, C. H. Lee, A. Iyo, H. Eisaki, K. Ohgushi, S. Kasahara, T. Terashima, H. Ikeda, T. Shibauchi, Y. Matsuda, and K. Ishizaka, Phys. Rev. B **89**, 045101 (2014).

[8] J. Maletz, V. B. Zabolotnyy, D. V. Evtushinsky, S. Thirupathaiah, A. U. B. Wolter, L. Harnagea, A. N. Yaresko, A. N. Vasiliev, D. A. Chareev, E. D. L. Rienks, B. Büchner, and S. V. Borisenko, Phys. Rev. B **89**, 220506(R) (2014).

[9] T. Shimojima, Y. Suzuki, T. Sonobe, A. Nakamura, M. Sakano, J. Omachi, K. Yoshioka, M. Kuwata-Gonokami, K. Ono, H. Kumigashira, A. E. Böhmer, F. Hardy, T. Wolf, C. Meingast, H. v. Löhneysen, H. Ikeda, and K. Ishizaka, Phys. Rev. B **90**, 121111(R) (2014).

[10] K. Nakayama, Y. Miyata, G. N. Phan, T. Sato, Y. Tanabe, T. Urata, K. Tanigaki, and T. Takahashi, arXiv:1404.0857

[11] H. Miao, L.-M. Wang, P. Richard, S.-F. Wu, J. Ma, T. Qian, L.-Y. Xing, X.-C. Wang, C.-Q. Jin, C.-P. Chou, Z. Wang, W. Ku, and H. Ding, Phys. Rev. B **89**, 220503(R) (2014).

[12] T. Sugimoto, D. Ootsuki, K. Sawada, H. Anzai, M. Arita, H. Namatame, M. Taniguchi, M. Horio, K. Horiba, M. Kobayashi, K. Ono, H. Kumigashira, T. Inabe, T. Noji, Y. Koike, N. L. Saini, and T. Mizokawa, arXiv:1411.0788.

[13] V. Cvetkovic and O. Vafek, Phys. Rev. B **88**, 134510 (2013).

[14] W. Z. Hu, J. Dong, G. Li, Z. Li, P. Zheng, G. F. Chen, J. L. Luo, and N. L. Wang, Phys. Rev. Lett. **101**, 257005 (2008).

[15] M. Nakajima, S. Ishida, K. Kihou, Y. Tomioka, T. Ito, Y. Yoshida, C. H. Lee, H. Kito, A. Iyo, H. Eisaki, K. M. Kojima, and S. Uchida, Phys. Rev. B **81**, 104528 (2010).

[16] M. Yi, Y. Zhang, Z.-K. Liu, X. Ding, J.-H. Chu, A. F. Kemper, N. Plonka, B. Moritz, M. Hashimoto, S.-K. Mo, Z. Hussain, T. P. Devereaux, I. R. Fisher, H. H. Wen, Z.-X. Shen, and D. H. Lu, Nature Comm. **5**, 3711 (2014).

[17] S. Borisenko, D. Evtushinsky, I. Morozov, S. Wurmehl, B. Büchner, A. Yaresko, T. Kim, and M. Hoesch, arXiv:1409.8669.

[18] R. S. Dhaka, S. E. Hahn, E. Razzoli, Rui Jiang, M. Shi, B. N. Harmon, A. Thaler, S. L. Bud'ko, P. C. Canfield, and A. Kaminski, Phys. Rev. Lett. **110**, 067002 (2013).

[19] V. Brouet, Ping-Hui Lin, Y. Texier, J. Bobroff, A. Taleb-Ibrahimi, P. Le Fèvre, F. Bertran, M. Casula, P. Werner, S. Biermann, F. Rullier-Albenque, A. Forget, and D. Colson, Phys. Rev. Lett. 110, 167002 (2013).

[20] O. K. Andersen and L. Boeri, Ann. Phys. **523**, 8 (2011).

[21] C.-H. Lin, T. Berlijn, L. Wang, C.-C. Lee, W.-G. Yin and W. Ku, Phys. Rev. Lett. **107**, 257001 (2011).

[22] M. Tomić, H. O. Jeschke, and R. Valentí, arXiv:1408.2258.

[23] Y. Wang, T. Berlijn, P. J. Hirschfeld, D. J. Scalapino, T. A. Maier, arXiv:1411.0070.

[24] We should mention, that without spin-orbit, each "doublet" has an additional two-fold spin degeneracy. This remnant degeneracy survives inclusion of either spin-orbit coupling or nematic, or both; such two-fold degeneracy is protected by the presence of time reversal symmetry and a center of space inversion[13]. Despite this additional degeneracy, we will continue referring to them as "doublets".

[25] C. J. Bradley and A. P. Cracknell, The Mathematical Theory of Symmetry in Solids (Clarendon, Oxford, 1972), pp.

131, 240, and 348.

[26] H. Eschrig and K. Koepernik, Phys. Rev. B **80**, 104503 (2009).

[27] To remove an artificial degeneracy of the 10-orbital tight-binding model of Ref.[26], and be consistent with the first-principle results, we added a small (symmetry allowed) nearest-neighbor hopping between the two z^2 orbitals in the unit cell, $2\tilde{t} \sum_{\mathbf{k}\sigma} c^{\dagger}_{z^2(1),\mathbf{k}\sigma} c_{z^2(2),\mathbf{k}\sigma} \left[\cos\left(\frac{k_x+k_y}{2}\right) + \cos\left(\frac{k_x-k_y}{2}\right) \right]$ with $\tilde{t} = -3$ meV.

[28] F. Krüger, S. Kumar, J. Zaanen, and J. van den Brink, Phys. Rev. B **79**, 054504 (2009).

[29] C. C. Lee, W. G. Yin, and W. Ku, Phys. Rev. Lett. **103**, 267001 (2009).

[30] C.-C. Chen, J. Maciejko, A. P. Sorini, B. Moritz, R. R. P. Singh, and T. P. Devereaux, Phys. Rev. B **82**, 100504 (2010).

[31] W. Lv and P. Phillips, Phys. Rev. B **84**, 174512 (2011).

[32] W.-C. Lee and P. W. Phillips, Phys. Rev. B **86**, 245113 (2012).

[33] S. Onari H. and Kontani, Phys. Rev. Lett. **109**, 137001 (2012).

[34] V. Stanev and P. B. Littlewood, Phys. Rev. B **87**, 161122(R) (2013).

[35] Z. Wang and A. H. Nevidomskyy, arXiv:1408.1408.

[36] C. Fang, H. Yao, W.-F. Tsai, J. Hu, and S. A. Kivelson, Phys. Rev. B **77**, 224509 (2008).

[37] C. Xu, M. Muller, and S. Sachdev, Phys. Rev. B **78**, 020501(R) (2008).

[38] R. M. Fernandes, A. V. Chubukov, J. Knolle, I. Eremin, and J. Schmalian, Phys. Rev. B **85**, 024534 (2012).

[39] S. Liang, A. Moreo, and E. Dagotto, Phys. Rev. Lett. **111**, 047004 (2013).

[40] J. Kang, A. F. Kemper, and R. M. Fernandes, arXiv:1406.2388